Journal of Sound and Vibration (1997) **199**(5), 751–776

GLOBAL ATTENUATION OF RANDOM VIBRATIONS IN A TAPERED AND SWEPT PANEL

J. D'CRUZ†

Defence Science and Technology Organisation, Aeronautical and Maritime Research Laboratory, P.O. Box 4331, *Melbourne, Victoria* 3001, *Australia*

(*Received* 20 *June* 1995, *and in final form* 21 *June* 1996)

The thin panels used in many modern-day structures are often prone to vibrate at excessive amplitudes. Instead of suffering the weight penalties which may be associated with passive damping treatments, an approach which can make use of the computational power on board many of these structures is to dampen such vibrations actively. Piezoceramic strain actuators, because of their compact and lightweight nature, and because of their lack of a need for a supporting structure to provide reaction points, are ideally suited for such applications. A technique is presented herein for the design and implementation of two two-input–three-output multi-variable controllers which use two piezoceramic patches as actuators, and a further two such patches, as well as an accelerometer, as sensors. These controllers are implemented on a tapered and swept aluminium panel subject to random excitation, such that the first five modes are simultaneously observed and controlled. A technique that determines good locations for the sensors and actuators, based on the modes to be controlled, is employed. The results show that the controllers perform well with respect to spillover, robustness and non-linearities. Finally, the results of an accelerometer traverse are presented, demonstrating the global nature of the vibration attenuation achieved.

1. INTRODUCTION

In the interest of saving weight, many modern-day structures contain thin, unsupported panels. Such panels are often prone to vibrate at excessive amplitudes. One method of overcoming this problem is via the application of passive damping treatments. However, such an approach may negate the weight savings gained by using the thin panels in the first place.

In view of the computing power on board many of today's structures, a viable approach to the solution of this problem is to employ digital feedback control actively to dampen these vibrations. Patch-type piezoceramic strain actuators, because of their thin, unobtrusive and lightweight nature, their ability to induce significant strains in their host structure, and their lack of a need for a supporting structure to provide reaction points, are ideally suited for such applications.

Much research has been conducted in the past decade on the static and dynamic control of flexible structures using piezoelectric strain actuators and sensors. In this research, a considerable amount of attention has been devoted to beam-like structures. For example, in one of the earlier papers in the field, Bailey and Hubbard [1] analyze and experimentally demonstrate a polyvinylidene fluoride (PVDF) distributed-parameter piezoelectric active

† Present address: MP 305, Noise & Vibration Section, General Motors-Holden's Automotive Limited, 241 Salmon Street, Port Melbourne, VIC 3207, Australia.

0022–460X/97/050751 + 26 $25.00/0/sv960651

vibration damper for a cantilever beam. A controller was designed using Lyapunov's second method and compared to two negative velocity feedback controllers, one with constant gain, and the other with constant-feedback voltage and time-varying gain. To simplify the problem, only the fundamental bending mode was excited and subsequently controlled. This work is extended by Burke and Hubbard [2], who present an analysis of distributed actuator control of flexible beams with various boundary conditions and non-uniform spatial distributions of piezoelectric material, with the second method of Lyapunov again being used to derive the control laws. It is shown here that certain boundary conditions *require* non-uniform actuator spatial distributions to be controllable. The actuation, sensing and control of flexible beams with piezoelectric strain actuators receives further attention in references [3–6], with reference [6] also examining the interesting case of simultaneous sensing and actuation.

Plate and shell-like structures have also received some attention in this field. For instance, Tzou and Gadre [7] develop an analytical model for a shell with an embedded piezoelectric layer. A finite element approach is then adopted by Tzou and Tseng [8] to model the dynamic behaviour of such structures. Possible applications detailed in the literature have related to a variety of areas, including vibration reduction, and sound radiation and transmission. Dimitriadis and Fuller [9] undertake a theoretical investigation into the active control of sound transmission through, and radiation from, a vibrating plate with piezoelectric strain actuators bonded to its surface. Dimitriadis, Fuller and Rogers [10] develop an approximate dynamic model for the vibration response of a simply supported elastic rectangular plate excited by a piezoelectric patch of variable rectangular geometry. Silcox [11] provides details of an experimental investigation which controls the sound pressure levels in a cylindrical structure with these actuators. Fuller, Hansen and Snyder [12] experimentally study the active control, with a piezoceramic actuator, of sound radiation from a thin rectangular panel. D'Cruz [13] experimentally demonstrates the use of a single-input–single-output pole-placement controller in attenuating the vibrations in a randomly excited rectangular panel. References [14–17] provide details of more recent studies.

Also reported in the literature are details of the distributed control of aerodynamically induced vibrations. Nitzche and Breitbach [18] analyze the possibility of helicopter rotor blade vibration attenuation with embedded lead zirconate titanate (PZT) actuators. Linear Quadratic Gaussian (LQG) and adaptive control schemes are evaluated, with the conclusion that the latter is necessary in order to cope with the variations in system characteristics with the blade position. Controller saturation problems occur when the control of higher modes is attempted, and/or when higher aerodynamic loadings are encountered. Heeg [19] presents an analytical investigation and experimental demonstration of wing-flutter suppression using piezoceramic actuators mounted on the wing support mechanism. Single-input–single-output control utilising gain feedback design was employed. Further investigations are under way at the NASA Langley Research Center and the Massachusetts Institute of Technology in which flutter suppression is to be achieved with an array of piezoceramic actuators embedded in the wing structure itself. Finally, Scott and Weisshaar [20] present a study of the use of piezoelectric actuators in the suppression of supersonic panel flutter with Linear Quadratic Regulator (LQR) controller design.

In the work described below, two two-input–three-output pole-placement controllers which use strain and acceleration feedback to determine the two piezoceramic strain actuation voltages are designed and tested on a tapered and swept aluminium panel. The control design methodology separates the system into two loops, each with one input and two outputs. This control design technique represents an extension of that detailed in [21], in which two control loops were also separately designed. The advantage of using two

single-input–two-output loops instead of one multi-input–multi-output loop is that the controller design process is simplified, thereby providing a greater degree of physical insight into the problem. Furthermore, such an approach does not necessarily result in a system with inferior design properties [22].

The panel is clamped along one edge and excited randomly by a loudspeaker such that at least its first five modes respond. The first five of these modes are subsequently observed and controlled. A method which determines good locations for each of the three sensors and two actuators, based on the shapes of the first five normal modes, is presented, as are results of an accelerometer traverse, which demonstrates that global attenuation is achieved. The results presented also show the controller to possess the desirable properties of lack of spillover, robustness to signal drift and saturation, and insensitivity to non-linearities.

2. TEST STRUCTURE

The geometry of the tapered and swept panel used to perform the experiment is illustrated in Figure 1. As may be seen, four piezoceramic patches in total were employed, two as actuators and two as sensors. Each patch, composed of PZT, had dimensions of 64 mm $\times$ 38 mm $\times$ 0·2 mm. The signal from the accelerometer was also used for feedback, thereby giving the plant two inputs and three outputs, with a mixture of collocated and non-collocated actuators and sensors. A loudspeaker, positioned approximately 30 mm from the panel, was used to excite at least the first five modes by providing band-limited random noise in the 3–100 Hz range.

3. SENSOR AND ACTUATOR LOCATIONS

It is important that each sensor and actuator be placed in a location in which it is able to observe and control a designated mode, or set of modes. What follows is an account of the reasoning employed to determine good locations for the sensors and actuators with this condition in mind.

The PZT patches respond to and impart a quantity which is proportional to the sum of principal strains or, namely, the *bulk strain*, while the accelerometer, at a particular frequency of (sinusoidal) excitation, has an output signal amplitude proportional to its displacement amplitude. It is hence important to determine the displacement field, and the distribution of bulk strains, over the panel. This was done by building a dynamic finite element model of the panel. As the panel is lightly damped, the model did not incorporate any damping. In Figure 2 are shown, for the first five normal modes, the contour plots

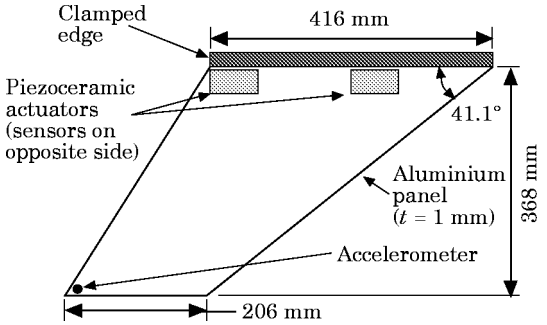

Figure 1. The test structure.

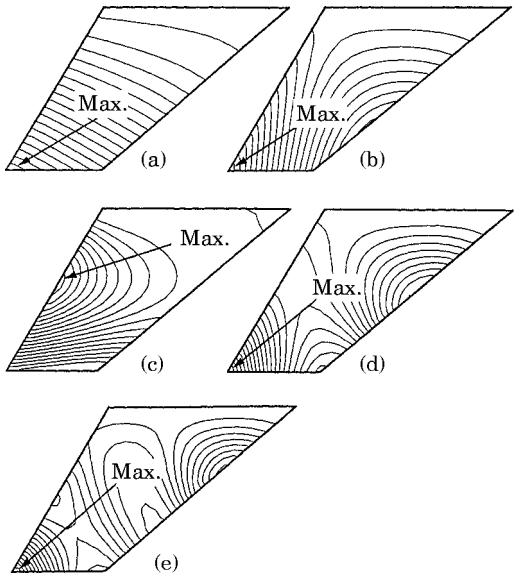

Figure 2. The displacement contours. (a) Mode 1, 5·6 Hz; (b) mode 2, 19·9 Hz; (c) mode 3, 35·5 Hz; (d) mode 4, 49·3 Hz; (e) mode 5, 84·9 Hz.

of displacement thus obtained, with the maximum displacement contour indicated. The corresponding representation for the bulk strains is shown in Figure 3.

Reference to Figures 1 and 3 will then reveal that the PZT sensor and actuator at the top l.h.s. of the panel are in a region in which the bulk strain is a maximum for the first and third modes. Likewise, the PZT sensor and actuator near the top r.h.s. are in a region in which the bulk strain is maximized for the fourth and fifth modes. Because of the limit in the number of sensors and actuators, no PZT transducer was located in the area in which there was a peak in the bulk strain for the second mode. However, the PZT sensor and

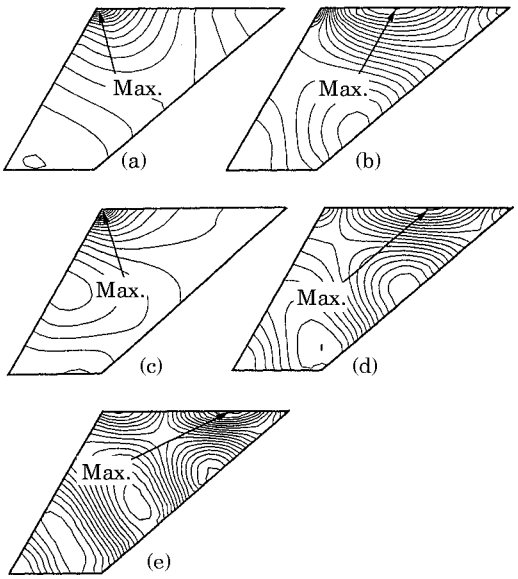

Figure 3. The bulk strain contours. Key as Figure 2.

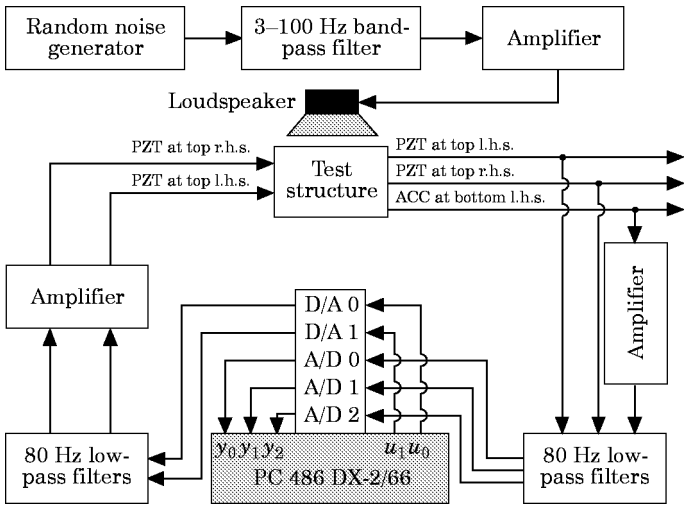

Figure 4. The experimental apparatus.

actuator near the top r.h.s. are in an area in which the bulk strain for mode 2 is relatively high, and should therefore be in good locations to observe and control that mode.

As far as the accelerometer is concerned, in Figures 1 and 2 it is shown that it is located in a region in which the acceleration is maximized for modes 1, 2, 4 and 5. Although it is *not* located in the area in which the acceleration is a maximum for the third mode, it is located is a region in which the acceleration levels for that mode are still high. It should consequently also be in a good location to observe the third mode.

4. EXPERIMENTAL APPARATUS

A schematic of the equipment used to implement the two-input–three-output controller is shown in Figure 4. It will be seen that low-pass filters were employed. This avoided aliasing of the output signals and removed the high frequency components present in the input signals, which were comprised of zero order holds. It will also be seen that only one amplifier (for the accelerometer) was used for the output signals. This was because the raw signals from the PZT sensors were of sufficient amplitude so as not to require amplification.

5. SYSTEM IDENTIFICATION AND CONTROL LAW DESIGN

The system illustrated in Figure 4 may be modelled by two loops, one within the other, each with one input and two outputs. This technique was also used in reference [21], with the important difference that each loop therein was a single-input–single-output one.

Now, each of the one-input–two-output loops may be represented by the "black-box" system shown in Figure 5, and by the corresponding discrete-time linear difference equations

$$\mathbf{y}(t) + a_1\mathbf{y}(t-1) + \cdots + a_{n_a}\mathbf{y}(t-n_a) = \mathbf{B}_1 u(t-1) + \cdots + \mathbf{B}_{n_b} u(t-n_b) + \mathbf{e}(t) \quad (1)$$

and

$$u(t) + f_1 u(t-1) + \cdots + f_{n_f} u(t-n_f) = -[\mathbf{G}_0\mathbf{y}(t) + \mathbf{G}_1\mathbf{y}(t-1) + \cdots + \mathbf{G}_{n_g}\mathbf{y}(t-n_g)]. \quad (2)$$

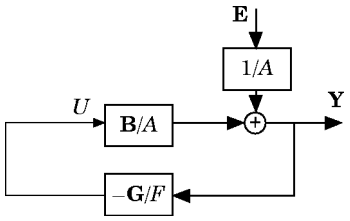

Figure 5. The loop block diagram.

(The variables appearing in Figure 5 are the z-transforms of those in equations (1) and (2).) If each of these loops shares only one sensor, the resulting system will have two inputs and three outputs. The unknown coefficients a_i, $\mathbf{B}_i$, f_i and $\mathbf{G}_i$ for each loop are determined as follows.

For each one-input–two-output loop define the parameter vector $\boldsymbol{\theta}$ as

$$\boldsymbol{\theta} = [a_1 \ldots a_{n_a}\, b_{11_1} \quad b_{21_1} \ldots b_{11_{n_b}} \quad b_{21_{n_b}}]^{\mathrm{T}}, \tag{3}$$

and the regression vectors $\boldsymbol{\psi}_1(t)$ and $\boldsymbol{\psi}_2(t)$ as

$$\boldsymbol{\psi}_1(t) = [-y_1(t-1) \ldots -y_1(t-n_a) \quad u(t-1) \ldots u(t-n_b)]^{\mathrm{T}}$$

and

$$\boldsymbol{\psi}_2(t) = [-y_2(t-1) \ldots -y_2(t-n_a) \quad u(t-1) \ldots u(t-n_b)]^{\mathrm{T}}, \tag{4}$$

where $t = 1, \ldots, N$. Minimization of the objective function

$$S_c = \frac{1}{2N} \sum_{t=1}^{N} \{[\, y_1(t) - \boldsymbol{\psi}_1^{\mathrm{T}}(t)\boldsymbol{\theta}_1]^2 + [\, y_2(t) - \boldsymbol{\psi}_2^{\mathrm{T}}(t)\boldsymbol{\theta}_2]^2\}, \tag{5}$$

where

$$\boldsymbol{\theta}_1 = [a_1 \ldots a_{n_a}\, b_{11_1} \ldots b_{11_{n_b}}]^{\mathrm{T}} \qquad \text{and} \qquad \boldsymbol{\theta}_2 = [a_1 \ldots a_{n_a}\, b_{21_1} \ldots b_{21_{n_b}}]^{\mathrm{T}},$$

results in the following least-squares estimate for the parameter vector:

$$\hat{\boldsymbol{\theta}}_N^{LS} = \left[\sum_{t=1}^{N} \left\{ \begin{bmatrix} \mathbf{L}_1(t) \\ \mathbf{R}_1(t) \end{bmatrix} [\mathbf{L}_1^{\mathrm{T}}(t) \quad \mathbf{R}_1^{\mathrm{T}}(t)] + \begin{bmatrix} \mathbf{L}_2(t) \\ \mathbf{R}_2(t) \end{bmatrix} [\mathbf{L}_2^{\mathrm{T}}(t) \quad \mathbf{R}_2^{\mathrm{T}}(t)] \right\} \right]^{-1}$$

$$\times \left[\sum_{t=1}^{N} \left\{ \begin{bmatrix} \mathbf{L}_1(t) \\ \mathbf{R}_1(t) \end{bmatrix} y_1(t) + \begin{bmatrix} \mathbf{L}_2(t) \\ \mathbf{R}_2(t) \end{bmatrix} y_2(t) \right\} \right] \tag{6}$$

where

$$\mathbf{L}_1 = [-y_1(t-1) \ldots \; -y_1(t-n_a)]^{\mathrm{T}}, \qquad \mathbf{L}_2 = [-y_2(t-1) \ldots \; -y_2(t-n_a)]^{\mathrm{T}},$$

$$\mathbf{R}_1 = [u(t-1)\, 0 \ldots u(t-n_b)\, 0]^{\mathrm{T}}, \qquad \mathbf{R}_2 = [0\, u(t-1) \ldots 0\, u(t-n_b)]^{\mathrm{T}}.$$

This estimate will be unbiased if the assumption that the noise $\mathbf{e}(t)$ is white is satisfied. Therefore, if a spectrally rich known signal u is used to excite the system and the responses y_1 and y_2 are recorded, equation (6) may be used to estimate the system coefficients, namely a_i and $\mathbf{B}_i$.

It will be noted from equation (5) that the two terms comprising the r.h.s. of the objective function were equally weighted. If, after computing $\hat{\boldsymbol{\theta}}_N^{LS}$ from equation (6), the two terms

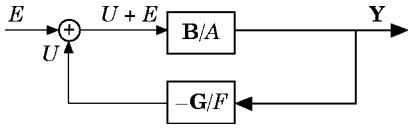

Figure 6. An alternative loop block diagram.

prove to be non-identical, the estimator will not have the minimum variance and is then deemed to be not *efficient*. To ensure that an unbiased and efficient value or, alternatively, the Minimum Variance Unbiased Estimator (MVUE), of $\boldsymbol{\theta}$ is obtained, the following procedure could have been adopted:

(1) Determine $\hat{\boldsymbol{\theta}}_N^{LS}$ from equation (6).
(2) Compute $\mu = [\Sigma_{t=1}^{N} (\, y_1(t) - \boldsymbol{\psi}_1^{\mathrm{T}}(t)\hat{\boldsymbol{\theta}}_1)^2]/[\Sigma_{t=1}^{N} (\, y_2(t) - \boldsymbol{\psi}_2^{\mathrm{T}}(t)\hat{\boldsymbol{\theta}}_2)^2]$.
(3) Define $\tilde{S}_c = (1/2N)\, \Sigma_{t=1}^{N} \{[\, y_1(t) - \boldsymbol{\psi}_1^{\mathrm{T}}(t)\boldsymbol{\theta}_1]^2 + \mu[\, y_2(t) - \boldsymbol{\psi}_2^{\mathrm{T}}(t)\boldsymbol{\theta}_2]^2\}$.
(4) Minimize $\tilde{S}_c$ to obtain $\hat{\boldsymbol{\theta}}$.
(5) Return to step (2).

When the parameter μ has converged, the estimator will be the MVUE; in other words, if the observations are weighted according to the inverse of their variances, the resulting estimator is the MVUE. The interested reader is referred to Ljung [23] for the proof and for a comprehensive description of the statistical properties of the least-squares estimate.

Although this iterative procedure was *not* adopted, the unbiased estimate for $\boldsymbol{\theta}$ obtained from equation (5), when subsequently employed to develop the controllers tested in this work, resulted in good vibration attenuation. This will be seen from the experimental results presented later.

It now remains to determine the coefficients f_i and $\mathbf{G}_i$, the controller gains. The approach used in this paper falls under the general description of *pole placement*. It is, because of the presence of multiple outputs, somewhat more involved than that detailed in reference [21]. However, because each loop has only a single input, solving for the controller gains is still possible with linear algebraic techniques.

Figure 5 may alternatively be represented by the more conventional control systems block diagram of Figure 6, where $\mathbf{B}\varepsilon(t) = \mathbf{e}(t)$. It then follows that

$$\mathbf{Y} = F[AF\,\mathbf{I} + \mathbf{BG}]^{-1}\mathbf{B}E, \tag{7}$$

which, for the one-input–two-output loop presently under consideration, gives

$$\mathbf{Y} = \frac{F[B_{11}B_{21}]^{\mathrm{T}}}{H}\,E, \tag{8}$$

where

$$H = H(z^{-1}) = A(z^{-1})F(z^{-1}) + B_{11}(z^{-1})G_{11}(z^{-1}) + B_{21}(z^{-1})G_{12}(z^{-1}). \tag{9}$$

The closed loop poles are therefore given by the zeros of $H(z^{-1})$, the closed loop characteristic polynomial.

In the approach detailed in reference [21], it was possible uniquely to determine the controller gains by specifying the locations of a number of closed loop poles, which was equal to the degree of the corresponding closed loop denominator polynomial. In the case under consideration here, this is no longer possible. For example, with $n_a = n_b = n_f = n_g + 1$,† pole assignment results in $2n_a$ equations with a total of $3n_a$ controller gains to be determined.

† Assume this to be the case from this point onward.

These $2n_a$ equations are formed as follows. If $2n_a$ closed loop poles are chosen such that they represent the roots of the equation

$$z^{2n_a} + r_1 z^{2n_a - 1} + \cdots + r_{2n_a} = 0, \tag{10}$$

the l.h.s of this equation may be equated to $z^{2n_a} H(z^{-1})$. This yields the $2n_a$ equations

$$[\mathbf{S}_a \; \mathbf{S}_{b_{11}} \; \mathbf{S}_{b_{21}}]\mathbf{c} = \mathbf{r}, \tag{11}$$

where

$$\mathbf{S}_a = \begin{bmatrix} 1 & 0 & \cdots & 0 \\ a_1 & 1 & \cdots & 0 \\ \vdots & \vdots & \ddots & \vdots \\ a_{n_a-1} & a_{n_a-2} & \cdots & \vdots \\ a_{n_a} & a_{n_a-1} & \cdots & \vdots \\ 0 & a_{n_a} & \cdots & \vdots \\ \vdots & \vdots & \ddots & \\ 0 & 0 & \cdots & a_{n_a-1} \\ 0 & 0 & \cdots & a_{n_a} \end{bmatrix},$$

and

$$\mathbf{S}_{b_{ij}} = \begin{bmatrix} b_{ij_1} & 0 & \cdots & 0 \\ b_{ij_2} & b_{ij_1} & \cdots & 0 \\ \vdots & \vdots & \cdots & \vdots \\ b_{ij_{n_b}} & b_{ij_{n_b-1}} & \cdots & \vdots \\ 0 & b_{ij_{n_b}} & \cdots & \vdots \\ 0 & 0 & \cdots & \vdots \\ \vdots & \vdots & \ddots & \vdots \\ 0 & 0 & \cdots & b_{ij_{n_b}} \\ 0 & 0 & \cdots & 0 \end{bmatrix},$$

$$\mathbf{c} = [f_1 \ldots f_{n_f} \quad g_{11_0} \ldots g_{11_{ng}} \quad g_{12_0} \ldots g_{12_{n_g}}]^{\mathrm{T}}$$

and

$$\mathbf{r} = [(r_1 - a_1) \ldots (r_{n_a} - a_{n_a}) \quad r_{n_a-1} \cdots r_{2n_a}]^{\mathrm{T}}.$$

The pole assignment problem may now be solved by additionally minimizing the objective function

$$S_g = \tfrac{1}{2}\left[\sum_{i=1}^{n_f} K_i f_i^2 + \sum_{i=0}^{n_g} (K_{11_i} g_{11_i}^2 + K_{12_i} g_{12_i}^2)\right] + \lambda_1 l_1 + \cdots + \lambda_{2n_a} l_{2n_a}, \tag{12}$$

where $\lambda_1, \ldots, \lambda_{2n_a}$ are unknown coefficients and $l_1, \ldots, l_{2n_a}$ are the expressions obtained from each of the $2n_a$ l.h.s.'s of equations (11) after transferring all terms on the corresponding r.h.s there. This is equivalent to minimizing a weighted sum of the squares of the controller gains subject to equations (11), which define the pole placements, being satisfied ($\lambda_1, \ldots, \lambda_{2n_a}$ are the Lagrange multipliers—see, for example [24]). The minimization is performed by satisfying the condition $\partial S_g/\partial f_1 = \cdots = \partial S_g/\partial g_{12_{n_g}} = 0$. Although $2n_a$ further unknowns (the Lagrange multipliers) are introduced, $3n_a$ additional equations can be formed. The problem now becomes one with $5n_a$ equations and $5n_a$ unknowns:

$$\mathbf{A}\mathbf{x} = \mathbf{b}, \tag{13}$$

where

$$\mathbf{A} = \begin{bmatrix} \mathbf{P} & \mathbf{0} \\ \mathbf{Q} & \mathbf{P}^{\mathrm{T}} \end{bmatrix}, \qquad \mathbf{x} = [\mathbf{c}^{\mathrm{T}} \quad \lambda_1 \ldots \lambda_{2n_a}]^{\mathrm{T}},$$

$$\mathbf{b} = \left[\mathbf{r}^{\mathrm{T}} \underbrace{0 \ldots 0}_{1+3n_a} \right]^{\mathrm{T}}, \qquad \mathbf{P} = [\mathbf{S}_{\mathrm{a}}\, \mathbf{S}_{b_{11}}\, \mathbf{S}_{b_{21}}]$$

and

$$\mathbf{Q} = \mathrm{diag}[K_1 \ldots K_{n_f} \quad K_{11_0} \ldots K_{11_{n_g}} \quad K_{12_0} \ldots K_{12_{n_g}}].$$

The following interpretation may be placed on the above-described minimization. Equation (2) may be written as

$$u(t) = -\sum_{i=1}^{n_f} f_i u(t-i) - \sum_{i=0}^{n_g} [g_{11_i} y_1(t-i) + g_{12_i} y_2(t-i)]. \tag{14}$$

Let there be disturbances to $u(t-i)$, $y_1(t-i)$ and $y_2(t-i)$, and represent these by $\delta u(t-i)$, $\delta y_1(t-i)$ and $\delta y_2(t-i)$ respectively. Then

$$\delta u(t) = -\sum_{i=1}^{n_f} f_i \delta u(t-i) - \sum_{i=0}^{n_g} [g_{11_i} \delta y_1(t-i) + g_{12_i} \delta y_2(t-i)]. \tag{15}$$

Assuming that the disturbances from one time interval to the next are uncorrelated, i.e., terms such as $\mathrm{E}[\delta u(t-i)\delta u(t-j)]_{i \neq j} = 0$, it follows that

$$\mathrm{E}[\delta u(t)]^2 = \sigma_u^2 \sum_{i=1}^{n_f} f_i^2 + \sum_{i=0}^{n_g} (\sigma_{y_1}^2 g_{11_i}^2 + \sigma_{y_2}^2 g_{12_i}^2), \tag{16}$$

where

$$\mathrm{E}[\delta u(t-i)^2] = \sigma_u^2, \qquad i = 1, \ldots, n_f,$$

$$E[\delta y_1(t-i)^2] = \sigma_{y_1}^2 \quad \text{and} \quad \mathrm{E}[\delta y_2(t-i)^2] = \sigma_{y_2}^2, \qquad i = 1, \ldots, n_g.$$

From equation (16) it may be seen that if the weighted sum of squares of the controller gains on the r.h.s is minimized, the effect of the above-mentioned disturbances on the computed control signal $u(t)$ is also minimized (cf., equation (12)).

Now, there are n_a open loop poles and $2n_a$ closed loop poles. If the n_a "excess" poles are assigned to the origin, it follows from equation (10) that $r_{n_a+1}, \ldots, r_{2n_a} = 0$. Hence,

from both equations (11) and (13), $f_{n_f} = 0$. In the light of this knowledge, equations (12) and (13) may respectively be recast in reduced form as

$$\bar{S}_g = \tfrac{1}{2}\left[\sum_{i=1}^{n_f-1} \bar{K}_i f_i^2 + \sum_{i=0}^{n_g} (\bar{K}_{11_i} g_{11_i}^2 + \bar{K}_{12_i} g_{12_i}^2)\right] + \bar{\lambda}_1 \bar{l}_1 + \cdots + \bar{\lambda}_{2n_a-1} \bar{l}_{2n_a-1}, \tag{17}$$

and

$$\bar{\mathbf{A}}\bar{\mathbf{x}} = \bar{\mathbf{b}}, \tag{18}$$

where

$$\bar{\mathbf{A}} = \begin{bmatrix} \bar{\mathbf{P}} & \mathbf{0} \\ \bar{\mathbf{Q}} & \bar{\mathbf{P}}^{\mathrm{T}} \end{bmatrix}, \qquad \bar{\mathbf{x}} = [\bar{\mathbf{c}}^{\mathrm{T}}\ \bar{\lambda}_1 \ldots \bar{\lambda}_{2n_a-1}]^{\mathrm{T}},$$

$$\bar{\mathbf{b}} = \left[(r_1 - a_1) \ldots (r_{n_a} - a_{n_a}) \underbrace{0 \ldots 0}_{1 \times (4n_a-2)}\right]^{\mathrm{T}}, \qquad \bar{\mathbf{P}} = [\bar{\mathbf{S}}_a\ \bar{\mathbf{S}}_{b_{11}}\ \bar{\mathbf{S}}_{b_{21}}],$$

$$\bar{\mathbf{Q}} = \mathrm{diag}[\bar{K}_1 \ldots \bar{K}_{n_f-1} \quad \bar{K}_{11_0} \ldots \bar{K}_{11_{n_g}} \quad K_{12_0} \ldots \bar{K}_{12_{n_g}}],$$

$$\bar{\mathbf{c}} = [f_1 \ldots f_{n_f-1} \quad g_{11_0} \ldots g_{11_{n_g}} \quad g_{12_0} \ldots g_{12_{n_g}}]^{\mathrm{T}},$$

$$\bar{\mathbf{S}}_a = \begin{bmatrix} 1 & 0 & \cdots & 0 \\ a_1 & 1 & \cdots & 0 \\ \vdots & \vdots & \ddots & \vdots \\ a_{n_a-1} & a_{n_a-2} & \cdots & \vdots \\ a_{n_a} & a_{n_a-1} & \cdots & \vdots \\ 0 & a_{n_a} & \cdots & \vdots \\ \vdots & \vdots & \ddots & \vdots \\ 0 & 0 & \cdots & a_{n_a} \end{bmatrix},$$

and

$$\mathbf{S}_{b_{ij}} = \begin{bmatrix} b_{ij_1} & 0 & \cdots & 0 \\ b_{ij_2} & b_{ij_1} & \cdots & 0 \\ \vdots & \vdots & \cdots & \vdots \\ b_{ij_{n_b}} & b_{ij_{n_b-1}} & \cdots & \vdots \\ 0 & b_{ij_{n_b}} & \cdots & \vdots \\ 0 & 0 & \cdots & \vdots \\ \vdots & \vdots & \ddots & \vdots \\ 0 & 0 & \cdots & b_{ij_{n_b}} \\ 0 & 0 & \cdots & 0 \end{bmatrix}.$$

Equation (18) may be solved by first partitioning $\bar{\mathbf{x}}$ and $\bar{\mathbf{b}}$ so that

$$\begin{bmatrix} \bar{\mathbf{P}} & \mathbf{0} \\ \bar{\mathbf{Q}} & \bar{\mathbf{P}}^{\mathrm{T}} \end{bmatrix} \begin{bmatrix} \bar{\mathbf{x}}_1 \\ \bar{\mathbf{x}}_2 \end{bmatrix} = \begin{bmatrix} \bar{\mathbf{b}}_1 \\ \bar{\mathbf{b}}_2 \end{bmatrix}, \tag{19}$$

where

$$\bar{\mathbf{x}}_1 = \bar{\mathbf{c}}, \qquad \bar{\mathbf{x}}_2 = [\bar{\lambda}_1 \ldots \bar{\lambda}_{2n_a - 1}]^{\mathrm{T}},$$

$$\bar{\mathbf{b}}_1 = \left[(r_1 - a_1) \ldots (r_{n_a} - a_{n_a}) \underbrace{0 \ldots 0}_{1 \times (n_a - 1)} \right]^{\mathrm{T}} \qquad \text{and} \qquad \bar{\mathbf{b}}_2 = \mathbf{0}_{(3n_a - 1) \times 1}.$$

Then $\bar{\mathbf{x}}_1$, the vector containing the $3n_a - 1$ controller coefficients or gains, is given by

$$\bar{\mathbf{x}} = \bar{\mathbf{Q}}^{-1} \bar{\mathbf{P}}^{\mathrm{T}} [\bar{\mathbf{P}} \bar{\mathbf{Q}}^{-1} \bar{\mathbf{P}}^{\mathrm{T}}]^{-1} \bar{\mathbf{b}}_1. \tag{20}$$

For non-zero weights, $\bar{\mathbf{Q}}$ will be invertible. Also, for all the cases considered, the inverse of $\bar{\mathbf{P}} \bar{\mathbf{Q}}^{-1} \bar{\mathbf{P}}^{\mathrm{T}}$ was found with no numerical difficulties.

6. EXPERIMENTAL RESULTS

The general approach, as already mentioned, is separately to design two one-input–two-output control loops with one sensor in common, thereby resulting in a system with two inputs and three outputs. First, a system identification was performed on one loop and a controller designed for it. *With this controller in operation*, a system identification was performed on the other loop, and another one-input–two-output controller was then designed. The two controllers were then operated simultaneously as a two-input–three-output controller to attenuate the panel vibrations.

The choice of sampling rate is an important one in controller design. In the problem under consideration here, it is a particularly difficult choice as the ratio of the highest predicted frequency to be controlled (84·9 Hz) to the lowest one (5·6 Hz) is more than 15:1. If the sampling rate is too low, there will be problems with controlling the higher modes, and if the sampling rate is too high, this problem occurs with the lower modes (in addition to the risk of exhausting the available computing resources). As a compromise, a sampling rate of 250 Hz was chosen which, as will be seen from the results presented later in this paper, led to good controller performance, with all the five modes of interest being controllable.

Referring again to Figure 1, the actuator for the first, or inner, loop was chosen to be the PZT patch at the top l.h.s. The sensors for this loop were (1) the PZT patch directly on the opposite side of the panel to the actuator, and (2) the accelerometer shown in Figure 1 at the bottom l.h.s. A random signal was then generated by the PC 486 DX-2/66 computer shown in Figure 4 and fed, via an 80 Hz low-pass filter and an amplifier, into the PZT actuator. The resulting sensor responses were filtered by the 80 Hz low-pass filters shown (only the accelerometer signal required pre-amplification) and fed into the analog-to-digital converters: 10 000 uniformly distributed random numbers were generated and output at the 250 Hz sampling rate. All this enabled equation (6) to be employed to determine the parameter vector $\boldsymbol{\theta}$ for this loop.

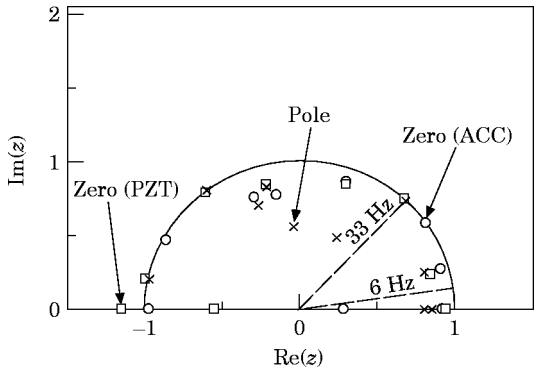

Figure 7. The open loop poles and zeros for the inner loop. Not plotted: PZT zeros at (−120·7, 0), (−1·299, 5·098), (−2·804, 0); ACC zeros at (−5·809, 0), (−4·593, 0), (−2·032, 2·315).

A model order of $n_a = n_b = 20$ was chosen. (A more formal technique for the choice of consistent order models is outlined in reference [21].) With this model order, the poles and zeros for this loop, given by the roots of

$$z^{n_a} + a_1 z^{n_a - 1} + \cdots + a_{n_a} = 0 \qquad \text{(poles)}$$

$$b_{11_1} z^{n_b - 1} + \cdots + b_{11_{n_b}} = 0 \qquad \text{(local zeros—PZT sensor)},$$

and

$$b_{21_1} z^{n_b - 1} + \cdots + b_{21_{n_b}} = 0 \qquad \text{(local zeros—ACCelerometer)}, \tag{21}$$

were plotted in Figure 7. The global zeros are obtained by combining both sets of local zeros. The first point of note in Figure 7 is that there exist global zeros outside the unit circle stability boundary. The system is consequently classed as *non-minimum phase*. This fact may only be due to the choice of sampling rate, with the continuous time system being minimum phase. However, it does exclude from consideration certain control design techniques—for instance, those which move poles to zeros. It will also be seen from Figure 7 that the poles at $0{\cdot}7966 \pm 0{\cdot}2437$i do not lie as close to the 6 Hz (mode 1)† frequency lines, as do those at $0{\cdot}6737 \pm 0{\cdot}7281$i to the 33 Hz (mode 3) frequency lines. This is because the former do not lie close to the unit circle in relation to the latter.

The pole-zero plot of Figure 7 may be converted to the continuous time transfer function plots of Figure 8 (see equation (5) of reference [21]). Even though, as previously mentioned, the poles at $0{\cdot}7966 \pm 0{\cdot}2437$i do not lie close to the mode 1 frequency lines, the overall pole-zero positions lead to peaks in the transfer function magnitude at 6·4 Hz and 4·0 Hz for y_0/u_0 and y_2/u_0 respectively, with the former peak being far more pronounced. The peak in magnitude for the latter, at this low frequency, is not as pronounced because the y_2/u_0 transfer function relates to acceleration, which is proportional, for sinusoidal motion at a particular amplitude, to the square of the frequency.

Having identified the inner open loop system, it is now possible to design a controller for it. As previously mentioned, the technique used for controller design was that of pole placement. Given a set of desired closed loop poles, equation (20) may be used to calculate the controller gains. However, in order to use this equation, it is also necessary to define

† As will be seen from results presented later in the paper, the first five modes were found to have measured frequencies of 6, 18, 33, 45 and 78 Hz respectively. These agree well with those found earlier by the finite element analysis, especially for the lower modes. For the higher modes, the predicted frequencies are higher than the measured ones because (1) the assumption of a clamped boundary is less valid, and (2) finite element models are generally stiffer than the structures they represent.

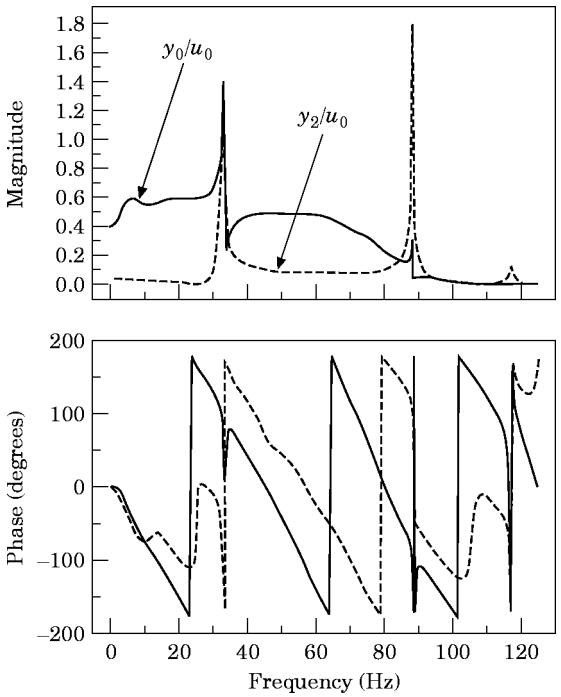

Figure 8. The open loop transfer functions for the inner loop. u_0, PZT; y_0, PZT; y_2, ACC.

the set of weights contained in the diagonal of matrix $\bar{\mathbf{Q}}$. There are a number of ways in which this may be done. One possibility is to weight the controller gains according to $\bar{\sigma}_u^2$, $\sigma_{y_1}^2$ and $\bar{\sigma}_{y_2}^2$, as defined in an equation similar to equation (16). Then the mentioned disturbance-rejection properties will be optimized. Alternatively, use could be made of the fact that, for high sampling rates, the poles of a sampled continuous system approach unity (see, for example, equation (1) of reference [25]). The weights may then be chosen based on the binomial coefficients obtained by expanding $(z-1)^n$. A third method weights the controller coefficients according to the reciprocals of their squared values, so that the gains make an equal contribution to the value of the objective function defined in equation (17). Because the values of the controller coefficients are not known *a priori*, an iterative scheme akin to the following may be used to implement this method of weight selection:

(1) Select an initial estimate for the weights.
(2) Compute the controller gains from equation (20).
(3) Assign the weights as reciprocals of squared controller gains.
(4) Repeat from step (2).

In fact, this was the method actually employed in the weight-selection process (the first of the above-mentioned methods requires $\bar{\sigma}_u^2$, $\bar{\sigma}_{y_1}^2$ and $\bar{\sigma}_{y_2}^2$ to be estimated—not a trivial task—while the second is not strictly valid unless the sampling rates chosen are actually much higher than the frequencies present in the system), and it resulted in good controller performance.

Before the third method was used, it was augmented by a number of features, as follows. (1) The initial estimates were unity for all the weights. (2) During the course of the iterative procedure, several of the controller gains converged to zero. If the weights were merely taken as the reciprocals of the squares of the gains, these weights would then

approach infinity. To avoid the numerical difficulties associated with this, a limit of $1/\varepsilon^2$ was placed on the weights, where ε was assigned a value of 10^{-6} times the average value of the magnitudes of the controller gains. (3) A limit of 15 was placed on the number of iterations performed. This number was sufficient to produce convergence in all the cases considered.

The PZT sensor and PZT actuator for the inner loop were placed so as to observe and control the first and third modes. The accelerometer was placed in a position which enabled it to observe the first five modes. Consequently, the poles for the first and third modes were moved along their respective constant frequency lines towards the origin and the controller gains calculated using equation (20) in conjunction with the iterative scheme just described. This has the effect, when the controller is implemented, of increasing the damping in these modes [21]. (Apart from assigning the previously referred to "excess poles" to the origin, the other poles were assigned to their stable open loop positions. While this ensures that they are stable, a pole assignment procedure without this restriction may indeed yield a smaller control effort. However, some means will have to be found to ensure that these poles do not cross the stability boundary, for instance, to move to the zeros outside the unit circle in this non-minimum phase system.)

In Figure 9 is shown the variation in r.m.s. control effort and the unfiltered sensor response with the prescribed increases in damping in the first and third modes. The sensor consists of an accelerometer located at the bottom r.h.s. of the panel illustrated in Figure 1 and is therefore *not* one of the feedback sensors. Test Point 1 corresponds to no increase in damping for both modes, while Test Point 11 corresponds to increases in damping by factors of 2·5 and 2·0 for modes 1 and 3 respectively, with linear variations in between. (The ranges of the damping increases considered were determined by examining the "control effort per unit increase in damping" for each mode separately.)

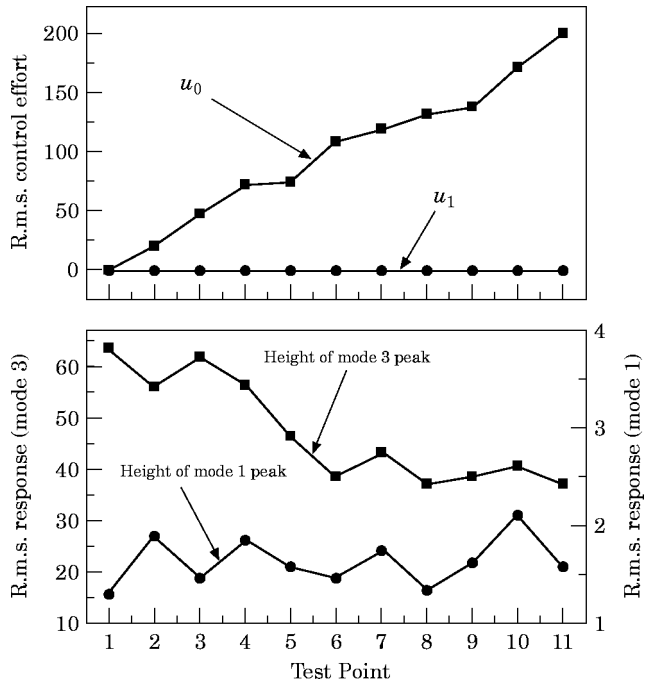

Figure 9. The r.m.s. control effort and response for various prescribed levels of inner-loop damping.

It is evident from Figure 9 that the height of the peak for mode 1 does not show a significant trend as the prescribed levels of damping are increased. This may be attributed to the fact that the pole corresponding to this mode is located well away from the unit circle, therefore implying that this mode is already relatively heavily damped. This is in contrast to the results for the height of the mode 3 peak, which decreases significantly with the prescribed increases in damping. The pole corresponding to mode 3, as was seen from Figure 7, is close to the unit circle, indicating light open loop damping. (It is easiest significantly to reduce the response of lightly damped modes.) A steady increase in the control effort for the one PZT actuator which is in use at this stage is also shown in Figure 9.

The choice of an optimal controller depends on the particular circumstances at hand. It is a function of not only the degree of vibration attenuation sought, but also of the cost of control energy. Furthermore, at the expense of greatly increasing the time required to perform the experiment (by incurring the so-called "curse of dimensionality"), a far greater number of combinations of prescribed damping for the two modes could have been examined in order to enable a more thorough optimization to be performed. Therefore, for the sake of illustration, Test Point 8 was chosen, where the damping for modes 1 and 3 were increased by factors of 2·05 and 1·7 respectively.

It was mentioned that the number of iterations in the control design procedure was limited to 15. In Figure 10 is shown the variation of the 59 controller gains $f_1, \ldots, f_{n_f-1}$, $g_{11_0}, \ldots, g_{11_{n_g}}$ and $g_{12_0}, \ldots, g_{12_{n_g}}$ with iteration number for the controller of Test Point 8. It may be seen that all these controller gains converged well before the 15-iteration limit. Also, several of the gains converged to zero. Use could have been made of this information, in addition to the fact that $f_{n_f} = 0$, to decrease the computation time required to implement the controller, should this have been a limiting factor.

Having designed the controller for the inner loop, it is now possible to design one for the outer loop. With reference to Figure 1, the PZT patch at the top r.h.s. was used as the actuator for the outer loop, with the PZT patch on the opposite side of the panel and the accelerometer on the bottom l.h.s. serving as the two sensors. This combination of sensors and actuators was, as previously discussed, chosen to observe and control the second, fourth and fifth modes.

With the inner-loop controller in operation, the characteristics of the outer loop were identified, again by first generating a uniformly distributed 10 000-number random

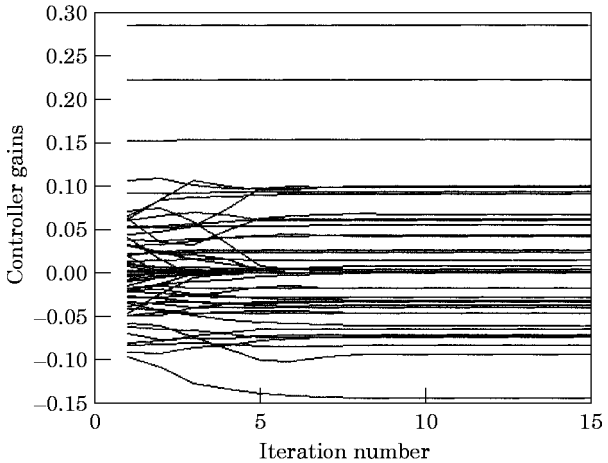

Figure 10. The progress of iterations for inner-loop controller gains.

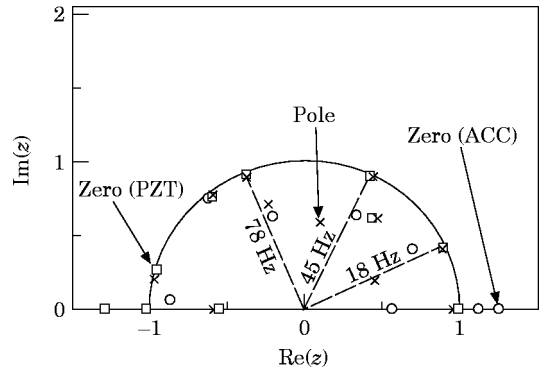

Figure 11. The poles and zeros for the outer loop. Not plotted: PZT zeros at (11·55, 13·61), (−5·123, 0·6430); ACC zeros at (−1·956, 1·909), (−1·059, 2·215), (−1·635, 0), (1·752, 0).

sequence and feeding it, via a second digital-to-analog converter, to the PZT actuator through the 80 Hz low pass filter and amplifier at a 250 Hz rate. The poles and zeros for the 20th order model employed to represent the outer loop appear in Figure 11, and the continuous-time transfer functions in Figure 12.

As for Figure 7, in Figure 11 it is shown that the system is non-minimum phase. Also to be noted from Figure 11 is the fact that the three sets of poles at $0{\cdot}9024 \pm 0{\cdot}4236$i, $0{\cdot}4324 \pm 0{\cdot}8975$i and $-0{\cdot}3714 \pm 0{\cdot}9200$i lie close to the 18 Hz (mode 2), 45 Hz (mode 4) and 78 Hz (mode 5) constant frequency lines respectively. These poles also lie close to the stability boundary, thereby illustrating the small amount of damping present in the corresponding modes. This leads to the sharp peaks seen in both the y_1/u_1 and y_2/u_1 magnitude curves of Figure 12.

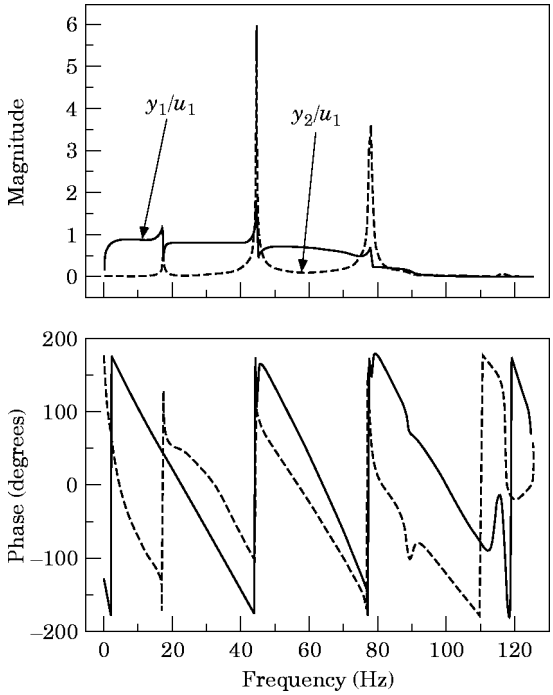

Figure 12. The transfer function for the outer loop. u_1, PZT; y_1, PZT; y_2, ACC.

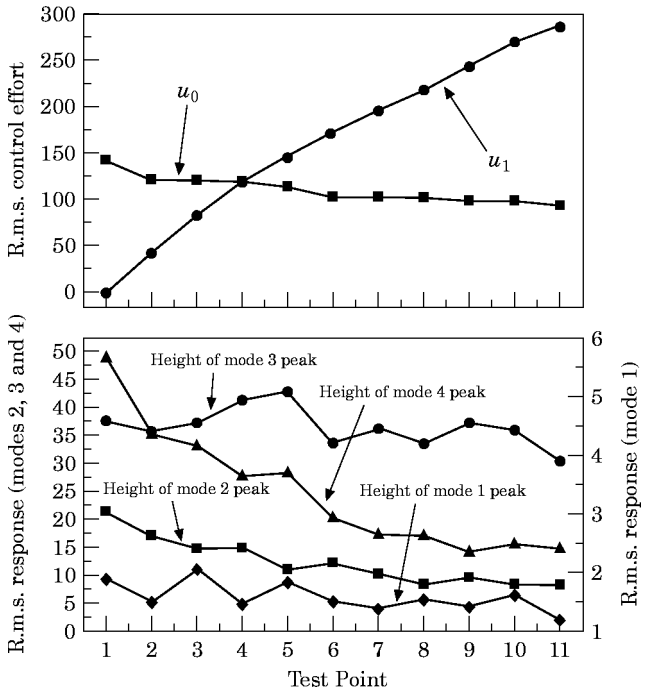

Figure 13. The r.m.s. control effort and response for various prescribed levels of outer-loop damping.

The second, or outer, loop having been identified, a controller may be designed for it. The modes being controlled by this controller are the second, fourth and fifth ones. Hence, in order to increase their damping, the poles corresponding to these modes were moved along their respective constant frequency lines toward the origin, with the other poles assigned to the origin and the open loop pole positions. In Figure 13 is shown the variation in the r.m.s. control effort and the unfiltered sensor response with the prescribed increases in the damping of these modes. Again, the sensor is an accelerometer located at the bottom r.h.s. of the panel. At Test Point 1 there is no increase in the damping prescribed to the three modes, while at Test Point 11 the damping of modes 2, 4 and 5 were prescribed to increase by factors of 2·25, 5·75 and 30 respectively, with linear variations in between. (The ranges of the damping increases considered were determined as for the inner loop.)

It will be seen from Figure 13 that the heights of the peaks for modes 2 and 4 both show significant decreases with the prescribed increases in damping. In addition, the peak for mode 5 effectively vanishes for *all* test points where there was some increase in damping prescribed. It will also be seen from Figure 13 that the height of the peaks corresponding to modes 1 and 3 also decrease with the increases in damping of modes 2, 4 and 5. This is evidence of some structural cross-coupling that is occurring between the inner and outer loops. Further evidence of this cross-coupling is that the r.m.s control effort for the inner-loop PZT actuator is actually *decreasing* with the prescribed increases in outer-loop damping. As expected, the r.m.s control effort for the outer-loop actuator instead exhibited a steady increase.

The reason for the inter-loop interaction is that the shapes of the modes under control are such that they cannot easily (if at all) be separated, so that they excite and respond to the sensors and actuator of only one loop. This is unlike the case of the rectangular panel discussed in reference [21], where some separation was readily accomplished.

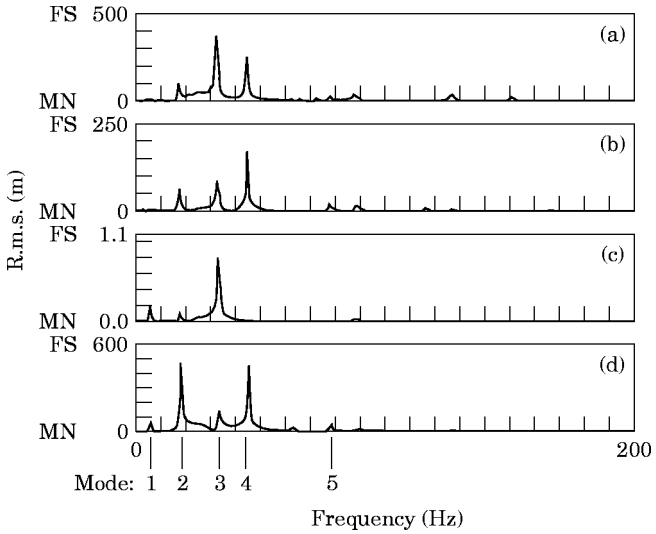

Figure 14. The unfiltered r.m.s. acceleration levels with the controller off. (a) ACC at bottom r.h.s.; (b) ACC at bottom l.h.s.; (c) PZT at top l.h.s.; (d) PZT at top r.h.s.

As for the inner loop, strict criteria were not used to choose the outer-loop controller. For illustrative purposes, two outer-loop controllers were chosen. The first corresponded to Test Point 3 and the second to Test Point 6. The prescribed increases in damping for modes 2, 4 and 5 were factors of 1·25, 1·95 and 6·8 (Test Point 3), and 1·875, 4·325 and 21·3 (Test Point 6) respectively. The first controller led to decreases in all the sensor feedback signals, while the second, although giving superior performance as far as reducing r.m.s. accelerations was concerned, led to a slight increase in the r.m.s. signal from the PZT sensor near the top r.h.s of Figure 1.

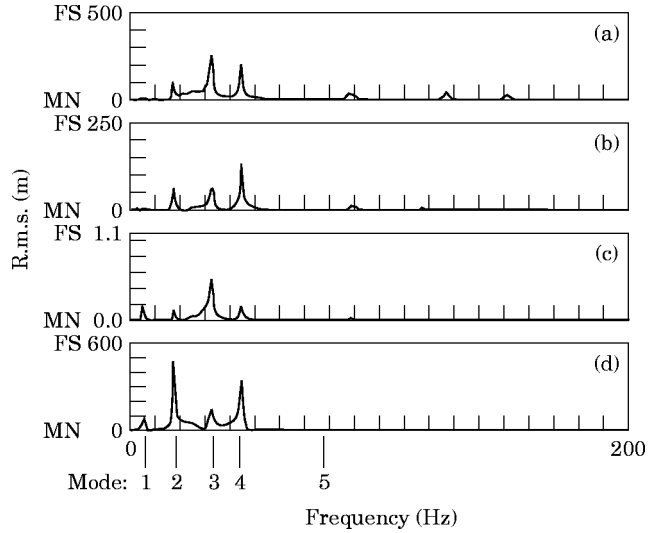

Figure 15. The unfiltered r.m.s. acceleration levels with the 2i3o controller on (outer loop, Test Point 3). Key as Figure 14.

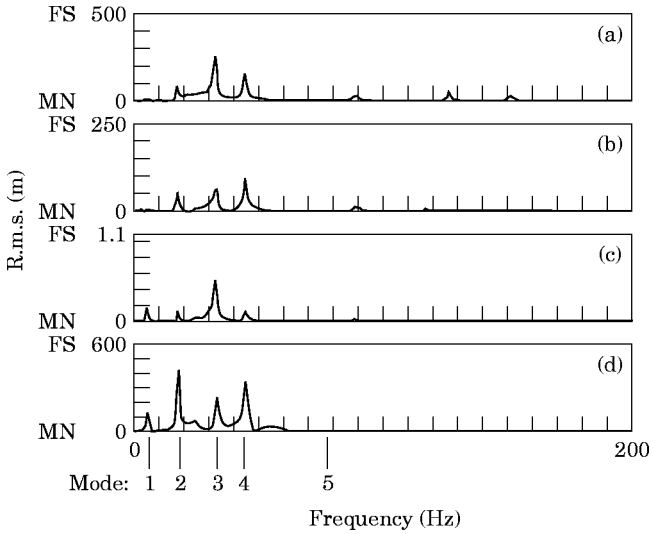

Figure 16. The unfiltered r.m.s. acceleration levels with the 2i3o controller on (outer loop, Test Point 6). Key as Figure 14.

As the iterative procedure used to determine them progressed, the behaviour of the outer-loop controller gains was similar to that exhibited for the inner-loop controller gains, with several of them again converging to zero.

In Figures 14–16 is shown the variation in the unfiltered r.m.s. signals of four sensors with frequency with the two-input–three-output controllers turned off and turned on. The first controller (inner loop, Test Point 8; outer loop, Test Point 3) produces a reduction in the r.m.s. of the (filtered) feedback sensor signals y_0 (PZT at top l.h.s.), y_1 (PZT at top r.h.s.) and y_2 (ACC at bottom l.h.s) of 13%, 4% and 19% respectively. The second controller (inner loop, Test Point 8; outer loop, Test Point 6) produces greater reductions in y_0 and y_2 (22% and 32% respectively) but gives a slight *increase* of 3% in y_1. As may be seen by comparing the lowermost plots of Figures 14 and 16, this is primarily due to energy from the first and third bulk-strain modes being transferred to the PZT sensor at the top r.h.s. In view of the decreases in the response levels, especially in the third mode, at the other sensor locations, the energy transfer is the result of a change in mode shapes, rather than an increase in modal responses.

A number of additional conclusions may be made from Figures 14–16. First, in Figures 15 and 16 it is shown that no spillover into the higher modes is evident. Second, in Figure 14 it is shown that all three feedback sensors (namely, the two PZT patches and the accelerometer at the bottom l.h.s.) were indeed located correctly by the method previously described. That is, the PZT sensor at the top l.h.s. sensed the first and third

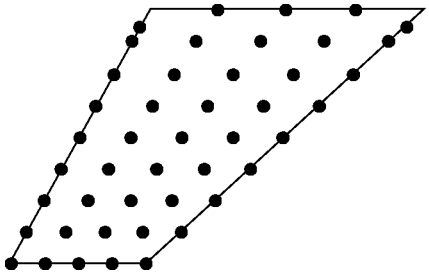

Figure 17. The positions of the accelerometer during the traverse.

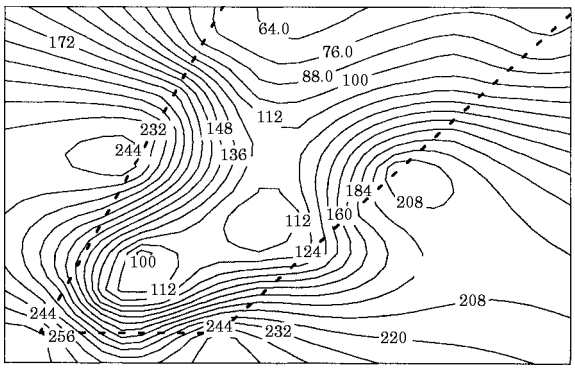

Figure 18. The r.m.s. acceleration contours with no control.

modes, the PZT sensor at the top r.h.s. the second, fourth and fifth modes, and the accelerometer at the bottom l.h.s. all five modes.

To demonstrate that reductions in vibration were achieved at other points on the panel, an accelerometer was traversed across it according to the grid illustrated in Figure 17. The r.m.s. of this unfiltered accelerometer signal, sampled at 5 kHz, with the no control and with each of the two-input–three-output controllers operating in turn was recorded at each of the grid points. These data were used to generate the contour plots of Figures 18–20.

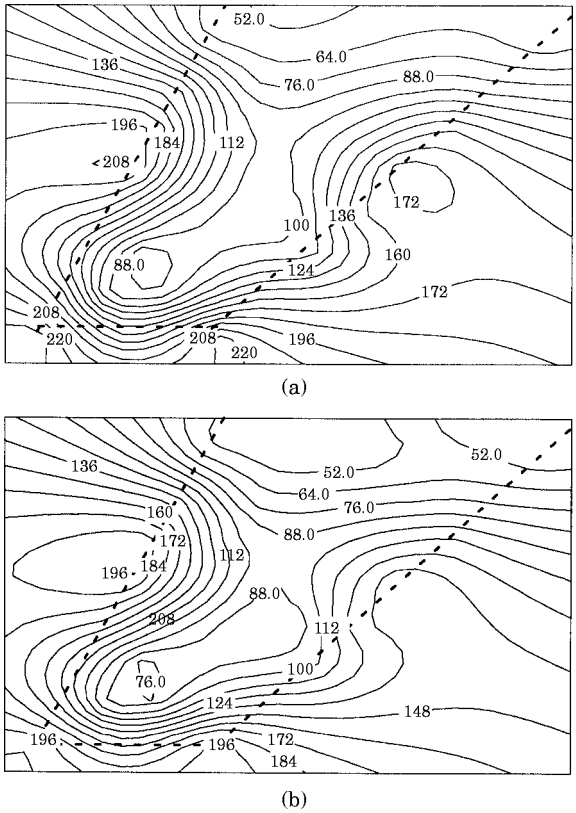

Figure 19. The r.m.s. acceleration contours with 2i3o control: (a) outer loop, Test Point 3; (b) outer loop, Test Point 6.

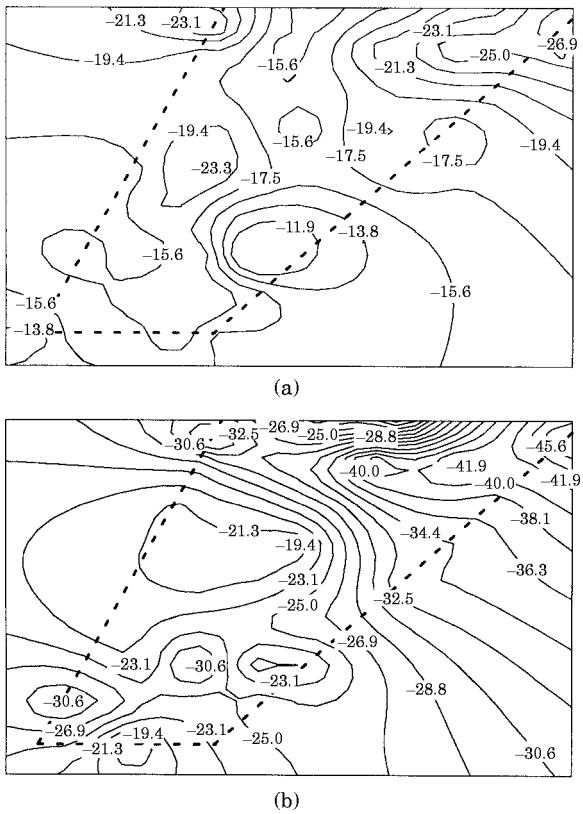

Figure 20. The percentage change in the r.m.s. acceleration: (a) outer loop, Test Point 3; (b) outer loop, Test Point 6.

From these plots it may be seen that *global reductions* in r.m.s. acceleration levels were produced by both controllers, with the second controller being more effective in this respect (in fact, a decrease due to control was registered at every grid point). The price paid for this increased effectiveness, however, is the slight increase in bulk strain seen by the PZT sensor near the top r.h.s. of the panel. The achievement of the goal of global vibration attenuation, as in reference [21], is a direct consequence of the fact that the poles were moved in such a manner as to increase the damping in the corresponding modes. This is a relatively easy task to accomplish with pole placement controllers.

Because of the way in which the panel was clamped, its low frequency vibrations led to a chatter-like phenomenon at the supported edge. This chattering in turn led to very high frequencies being present in the acceleration response, especially near the supported edge, as may be seen from Figures 21 and 22. Moreover, these plots show that both of the two-input–three-output controllers tested, by virtue of reducing the vibrations of the panel which were less than about 80 Hz (which they were designed to do), were also very successful in reducing the vibrations in the several-kilohertz range.

During testing, the controllers also exhibited good robustness properties. For instance, despite the fact that significant signal drifts were observed, the controllers continued to produce good attenuation in vibration levels. In addition, the controllers exhibited robustness to signal saturation.

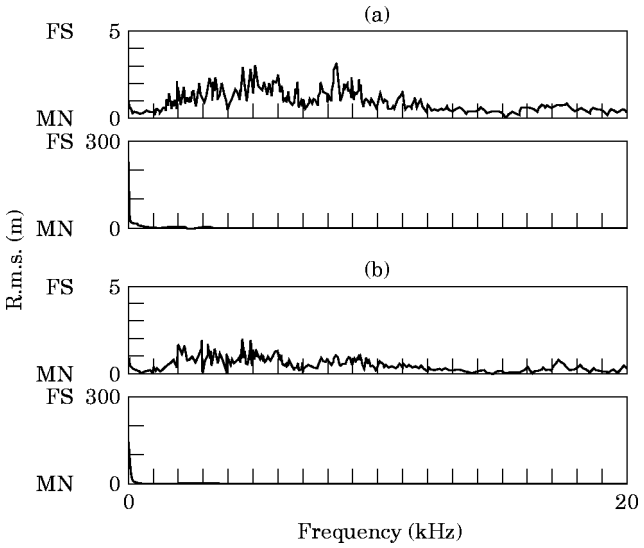

Figure 21. The high frequency behaviour of the 2i3o controller: outer-loop Test Point 3. (a) No control; (b) control. Within each part: upper graph, ACC at support; lower graph, ACC at tip.

7. DISCUSSION AND CONCLUSIONS

The design and synthesis of two two-input–three-output controllers which suppressed random vibrations in a tapered and swept aluminium panel were described above. Although the pole placement technique described is less complex than, for instance, the well-established Lyapunov or LQG methods, what resulted, when the controller was implemented, was the following: (1) no spillover into the higher modes was observed; (2) global reductions in vibration were produced; and (3) robustness to signal drift and saturation was demonstrated. Points (1) and (2) may be seen from the results presented above. Point (3) was observed during controller testing, when signal and saturation occurred intermittently but did *not* prevent the controller from significantly attenuating

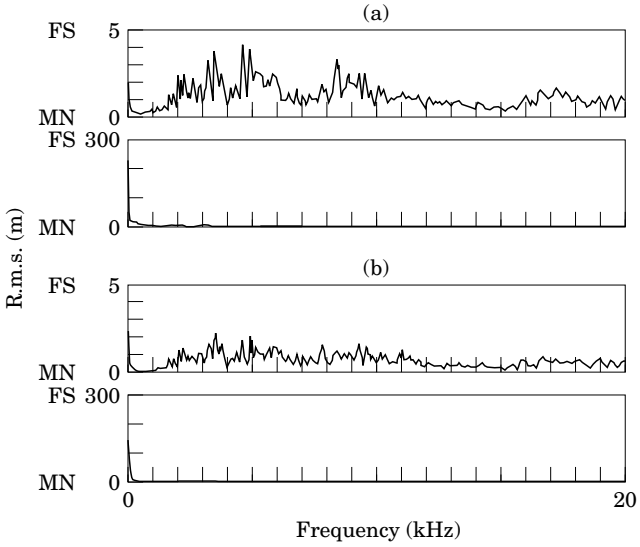

Figure 22. The high frequency behaviour of the 2i3o controller: outer-loop Test Point 6. Key as Figure 21.

the level of vibration. These three characteristics are indeed desirable and are not necessarily easy to obtain.

In the second and more effective of the two controllers tested, the bulk strain levels in one of the PZT feedback sensors was observed to increase slightly. This may have been overcome by using the flexibility in the above-described controller design technique to weight the readings from this sensor more heavily.

It was pointed out that, with the lowest frequency to be controlled predicted to be less than the highest frequency to be controlled by a factor of more that 15, the choice of sampling rate was a particularly difficult one. (This ratio actually turned out to be 13 for the measured frequencies.) As a compromise, a sampling rate of 250 Hz was settled upon. Although this was only 3·2 times the highest measured and controlled frequency of 78 Hz, the controllers still were able significantly to attenuate this mode, as was evident from measuring their performance at much higher sampling rates. Nevertheless, if the requirement had been to produce a "good" 78 Hz *waveform*, it may have not have been met so easily with a 250 Hz sampling rate.

Because of the non-linear behaviour of the panel support, excitation of the panel with 3–100 Hz random noise also produced a response in the several-kilohertz range. The frequency of the highest mode designed to be controlled was 78 Hz. By controlling this and the lower modes, the response up to several kilohertz was also attenuated significantly, thereby showing that the support non-linearities did not pose a problem.

In conclusion, it may therefore be stated that the above method for designing multi-variable controllers is more straightforward than some, and produced controllers with a good performance and some highly desirable properties. A possible avenue of further research is to determine the means by which these properties may be *guaranteed*. Other possible extensions to the above-described work are to determine if significant improvements in controller performance may be obtained by: (1) using the MVUE for system identification; (2) weighting the controller gains by the alternative techniques described; or (3) removing the constraint that some of the closed loop poles be assigned to their open loop positions.

ACKNOWLEDGMENTS

The author is grateful for the guidance provided by Dr T. G. Ryall and Mr P. A. Farrell with regard to the theoretical and practical aspects of this work. Acknowledgment is also due to Mr A. J. Barylko for writing the C routines which formed an interface between the author's FORTRAN programs and the real-time input/output board.

REFERENCES

1. T. Bailey and J. E. Hubbard, Jr. 1985 *Journal of Guidance, Control, and Dynamics* **8**, 605–611. Distributed piezoelectric-polymer Active vibration control of a cantilever beam.
2. S. E. Burke and J. E. Hubbard, Jr. 1988 *Automatica* **24**, 619–627. Distributed actuator control design for flexible beams.
3. E. F. Crawley and J. de Luis 1987 *American Institute of Aeronautics and Astronautics Journal* **25**, 1373–1385. Use of piezoelectric actuators as elements of intelligent structures.
4. I. Legrain 1990 *ONERA Activities* 1989, R-9–R-10. Paris: ONERA. Active vibration control by piezoelectric elements.
5. S. Devasia, T. Meressi, B. Paden and E. Bayo 1993 *Journal of Guidance, Control, and Dynamics* **16**, 859–864. Piezoelectric actuator design for vibration suppression: placement and sizing.
6. E. H. Anderson and N. W. Hagood 1994 *Journal of Sound and Vibration* **174**, 617–639. Simultaneous piezoelectric sensing/actuation: analysis and application to controlled structures.

7. H. S. TZOU and M. GADRE 1989 *Journal of Sound and Vibration* **132**, 433–450. Theoretical analysis of a multi-layered thin shell coupled with piezoelectric shell actuators for distributed vibration controls.
8. H. S. TZOU and C. I. TSENG 1990 *Journal of Sound and Vibration* **138**, 17–34. Distributed piezoelectric sensor/actuator design for dynamic measurement/control of distributed parameter systems: a piezoelectric finite element approach.
9. E. DIMITRIADIS and C. FULLER 1989 12*th Aeroacoustics Conference*, 89–1062. Investigation on active control of sound transmission through elastic plates using piezoelectric actuators.
10. E. K. DIMITRIADIS, C. R. FULLER and C. A. ROGERS 1989 *ASME* 8*th Biennial Conference on Failure Prevention and Reliability*, 223–233. Piezoelectric actuators for distributed noise and vibration excitation of thin plates.
11. R. J. SILCOX 1990 *NASA Technical Memorandum* 4243: *Research and Technology* 1990, 47. Noise control in fuselage structures using piezoceramic actuators.
12. C. R. FULLER, C. H. HANSEN and S. D. SNYDER 1991 *Journal of Sound and Vibration* **150**, 179–190. Experiments on active control of sound radiation from a panel using a piezoceramic actuator.
13. J. D'CRUZ 1993 *Journal of Intelligent Material Systems and Structures* **4**, 398–402. The active control of panel vibrations with piezoelectric actuators.
14. B.-T. WANG, R. A. BURDISSO and C. R. FULLER 1994 *Journal of Intelligent Material Systems and Structures* **5**, 67–77. Optimal placement of piezoelectric actuators for active structural acoustic control.
15. H. S. TZOU and H. Q. FU 1994 *Journal of Sound and Vibration* **172**, 247–259. A study of segmentation of distributed piezoelectric sensors and actuators, part I: theoretical analysis.
16. H. S. TZOU and H. Q. FU 1994 *Journal of Sound and Vibration* **172**, 261–275. A study of segmentation of distributed piezoelectric sensors and actuators, part II: parametric study and active vibration controls.
17. E. T. FALANGAS, J. A. DWORAK and S. KOSHIGOE 1994 *IEEE Control Systems* **14**, 34–41. Controlling plate vibrations using piezoelectric actuators.
18. F. NITZSCHE and E. BREITBACH 1992 1*st European Conference on Smart Structures and Materials*, 321–324. The smart structures technology in the vibration control of helicopter blades in forward flight.
19. J. HEEG 1993 *NASA Technical Paper* 3241. Analytical and experimental investigation of flutter suppression by piezoelectric actuation.
20. R. C. SCOTT and T. A. WEISSHAAR 1994 *Journal of Aircraft* **31**, 213–222. Panel flutter suppression using adaptive material actuators.
21. J. D'CRUZ 1995 *Journal of Intelligent Material Systems and Structures* **6,** 419–429. Global multivariable vibration control with distributed piezoceramic actuators.
22. G. F. FRANKLIN, J. D. POWELL and M. L. WORKMAN 1990 *Digital Control of Dynamic Systems*, 418. Reading, MA: Addison-Wesley.
23. L. LJUNG 1987 *System Identification: Theory for the User*, 469–476. Englewood Cliffs, N. J.: Prentice-Hall.
24. A. E. BRYSON, JR. and Y.-C. HO 1975 *Applied Optimal Control*, vol. 6. New York: Hemisphere.
25. K. J. ÅSTRÖM, P. HAGANDER and J. STERNBY 1984 *Automatica* **20**, 31–38. Zeros of sampled systems.

APPENDIX: NOMENCLATURE

a_i	coefficients of ARX model, $i = 1, \ldots, n_a$
A, $A(z^{-1})$	$= 1 + a_1 z^{-1} + \cdots + a_{n_a} z^{-n_a}$
$\mathbf{A}$	matrix formed from sub-matrices $\mathbf{P}$ and $\mathbf{Q}$ and defined in equation (13)
b_{ijk}	ijth component of $\mathbf{B}_k$, $i = 1, 2$, $j = 1$, $k = 1, \ldots, n_b$
$\mathbf{b}$	$= \left[\mathbf{r}^{\mathrm{T}} \underbrace{0 \ldots 0}_{1 \times 3n_a} \right]^{\mathrm{T}}$
$\bar{\mathbf{b}}_i$	components of $\bar{\mathbf{b}}$ defined in equation (19), $i = 1, 2$
B_{ij}, $B_{ij}(z^{-1})$	ijth component of $\mathbf{B}$, $i = 1$, $j = 1, 2$

$\mathbf{B}$, $\mathbf{B}(z^{-1})$	$=\mathbf{B}_1 z^{-1} + \cdots + \mathbf{B}_{n_b} z^{-n_b}$
$\mathbf{B}_i$	2×1 coefficient vectors of ARX model
$\mathbf{c}$	$=[f_1 \ldots f_{n_f}\, g_{11_0} \ldots g_{11_{n_g}}\, g_{12_0} \ldots g_{12_{n_g}}]^{\mathrm{T}}$ vector of controller coefficients or gains
$\mathbf{e}(t)$	white noise term of ARX model
E	z-transform of $\varepsilon(t)$
$\mathbf{E}$	z-transform of $\mathbf{e}(t)$
f_i	controller coefficients or gains, $i = 1, \ldots, n_f$
F, $F(z^{-1})$	$=1 + f_1 z^{-1} + \cdots + f_{n_f} z^{-n_f}$
g_{ij_k}	ijth component of $\mathbf{G}_k$, $i = 1$, $j = 1, 2$, $k = 0, \ldots, n_g$
G_{ij}, $G_{ij}(z^{-1})$	ijth component of $\mathbf{G}$, $i = 1$, $j = 1, 2$
$\mathbf{G}$, $\mathbf{G}(z^{-})$	$=\mathbf{G}_0 + \mathbf{G}_1 z^{-1} + \cdots + \mathbf{G}_{n_g} z^{-n_g}$
$\mathbf{G}_i$	1×2 controller coefficient or gain vector, $i = 0, \ldots, n_g$
H, $H(z^{-})$	$= AF + B_{11}G_{11} + B_{21}G_{12}$, characteristic polynomial of closed loop system
i	$=\sqrt{-1}$
$\mathbf{I}$	2×2 identity matrix
K_i	weight on f_i^2 in S_g, $i = 1, \ldots, n_f$
K_{ij_k}	weight of $g_{ij_k}^2$ in S_g, $i = 1$, $j = 1, 2$, $k = 0, \ldots, n_g$
l_i	expression obtained from l.h.s. of equation (11) after transfer of all terms from r.h.s.
$\mathbf{L}_1(t)$	$=[-y_1(t-1) \ldots -y_1(t-n_a)]^{\mathrm{T}}$
$\mathbf{L}_2(t)$	$=[-y_2(t-1) \ldots -y_2(t-n_a)]^{\mathrm{T}}$
n	power of binomial expansion
n_a	number of coefficients, a_i
n_b	number of coefficient vectors, $\mathbf{B}_i$
n_f	number of coefficients, f_i
n_g	number of coefficient vectors, $\mathbf{G}_i$, less 1
N	number of samples
$\mathbf{P}$	$=[\mathbf{S}_a\, \mathbf{S}_{b_{11}}\, \mathbf{S}_{b_{21}}]$
$\mathbf{Q}$	$=\mathrm{diag}[K_1 \ldots K_{n_f}\, K_{11_0} \ldots K_{11_{n_g}}\, K_{12_0} \ldots K_{12_{n_g}}]$, diagonal matrix of weights
r_i	coefficients of polynomial in z formed from $2n_a$ assigned closed loop poles $i = 1, \ldots, 2n_a$
$\mathbf{r}$	$=[(r_1 - a_1) \ldots (r_{n_a} - a_{n_a}) \quad r_{n_a+1} \ldots r_{2n_a}]^{\mathrm{T}}$
$\mathbf{R}_1(t)$	$=[u(t-1)\, 0 \ldots u(t-n_b)\, 0]^{\mathrm{T}}$
$\mathbf{R}_2(t)$	$=[0\, u(t-1) \ldots 0\, u(t-n_b)]^{\mathrm{T}}$
S_c	objective function for system identification
$\tilde{S}_c$	weighted (by μ) sum of variance of $\hat{\boldsymbol{\theta}}_1$ and variance of $\hat{\boldsymbol{\theta}}_2$
S_g	objective function, defined in equation (12)
$\mathbf{S}_a$, $\mathbf{S}_{b_{ij}}$	Sylvester matrices, defined in equation (11), $i = 1, 2$, $j = 1$
t	discrete time variable
u_i	digital value of control signal as sent to D/A converter j, $j = 0, 1$
$u(t-i)$	control variable at time $t - i$
U	z-transform of $u(t)$
$\mathbf{x}$	$=[\mathbf{c}^{\mathrm{T}} \quad \lambda_1 \ldots \lambda_{2n_a}]^{\mathrm{T}}$
$\bar{\mathbf{x}}_i$	components of $\bar{\mathbf{x}}$ defined in equation (19), $i = 1, 2$
y_i	sensor response as digitized by A/D converter i, $i = 0, 1, 2$
$y_j(t-i)$	jth component of $\mathbf{y}(t-i)$, $j = 1, 2$
y_i/u_j	transfer function representing response y_i due to excitation u_j, $i = 0, 1, 2$, $j = 0, 1$
$\mathbf{y}(t-i)$	2×1 system response vector at time $t - i$
$\mathbf{Y}$	z-transform of $\mathbf{y}(t)$
z^{-1}	backward shift operator
$\delta u(t-i)$	disturbance to $u(t-i)$, $i = 0, \ldots, n_f$
$\delta y_i(t-i)$	disturbance to $y_i(t-j)$, $i = 1, 2$ $j = 0, \ldots, n_g$
$\varepsilon(t)$	noise term defined by $\mathbf{B}\varepsilon(t) = \mathbf{e}(t)$
$\boldsymbol{\theta}$	$=[a_1 \ldots a_{n_a}\, b_{11_1}\, b_{12_1} \ldots b_{11_{n_b}}\, b_{21_{n_b}}]^{\mathrm{T}}$, parameter vector
$\boldsymbol{\theta}_i$	$=[a_1 \ldots a_{n_a}\, b_{i1_1} \ldots b_{i1_{n_b}}]^{\mathrm{T}}$, parameter vector
$\hat{\boldsymbol{\theta}}_N^{LS}$	least-squares estimate of parameter vector $\boldsymbol{\theta}$ with N samples
λ_i	Lagrange multiplier, $i = 1, \ldots, 2n_a$
μ	ratio of variance of $\hat{\boldsymbol{\theta}}_1$ to variance of $\hat{\boldsymbol{\theta}}_2$
σ_u^2, $\sigma_{y_i}^2$	expected values of $\delta u(t-i)^2$ and $\delta y_j(t-k)^2$, $i = 1, \ldots, n_f$, $j = 1, 2$, $k = 0, \ldots, n_g$
$\boldsymbol{\psi}_i(t)$	$=[-y_i(t-1) \ldots -y_i(t-n_a)\, u(t-1) \ldots u(t-n_b)]^{\mathrm{T}}$, regression vector

Accents and operators

$\bar{}$	denotes terms from reduced system
$\hat{}$	estimate
T	transpose
$\partial/\partial x$	partial derivative w.r.t. x
E	expected value